Physica 12D (1984) 32-44
North-Holland, Amsterdam

NUMERICAL SIMULATION OF TURBULENT MIXING BY RAYLEIGH–TAYLOR INSTABILITY

David L. YOUNGS
Atomic Weapons Research Establishment, Aldermaston, Berkshire, England

Two-dimensional hydrodynamic codes are used to simulate the growth of perturbations at an interface between two fluids of different density due to Rayleigh–Taylor instability. Problems where the interface is subjected to a constant acceleration and where it is accelerated and decelerated by shock waves are considered. Emphasis is placed on the case when the initial perturbation consists of many different wavelength modes. Results are compared with the experimental data of Andronov et al. (1976) and Read (1983). The use of a simple empirical model of the mixing process based on the equations of two-phase flow is discussed.

1. Introduction

Rayleigh–Taylor instability occurs when the interface between two fluids of different density is subjected to a normal pressure gradient with direction such that the pressure is higher in the light fluid than in the dense fluid, see, for example ref. 1. A related process occurs when shock waves pass through an interface. The small amplitude theory for this case was investigated by Richtmyer [2]; shock tube instability experiments were performed by Meshkov, see [3] and the references therein. As a result this process is often referred to as the Richtmyer–Meshkov instability.

Such instabilities are of current interest because of their deleterious effect on the performance of Inertially Confined Fusion (ICF) capsules, see [4] for example. Much of the previous theoretical work described in the review article [5] has concentrated on the growth of single wavelength perturbations. The main purpose of the present investigation is to study the growth of instabilities from random initial perturbations where many different wavelength modes are present. This situation is considered to be more relevant to practical applications. The complex flow that evolves should be regarded as an example of turbulent mixing and analysis of both computational and experimental results should involve measurement of the average properties of the mixed region.

Two-dimensional computer simulation using Eulerian hydrodynamics codes has been used to investigate the Rayleigh–Taylor and Richtmyer–Meshkov processes. This gives considerable insight into the behaviour of the large scale features of the mixed region. However, the real phenomena are three dimensional. For example the dissipation of turbulence kinetic energy by the transfer of energy to successively smaller and smaller eddies until viscous damping occurs, will certainly not be treated correctly in the two dimensional simulations. Three-dimensional simulation of the problems of most interest, where multiple wavelength initial perturbations are present was thought to be impractical using the computer facilities presently available at AWRE (a CRAY-1). Experimental studies, which are of course three dimensional were therefore considered to be essential. Rayleigh–Taylor instability experiments performed at AWRE are described by Read [6] and Read and Youngs [7]. Computational results for the Richtmyer–Meshkov process have been compared with the experimental data of Andronov et al. [3].

The understanding of the mixing processes achieved from computer simulation and experimental studies needs to be applied to practical prob-

lems. This article concludes with some thoughts on how this might be carried out. It is suggested that the equations of two-phase flow may be used to model the mixing process in a one-dimensional hydrocode. Such a technique could be used, for example, to predict the break up due to hydrodynamic instabilities of interfaces in ICF capsules.

2. Rayleigh–Taylor instability

2.1. *Basic picture of the mixing process*

Two incompressible fluids of densities ρ_1 and ρ_2 ($\rho_1 > \rho_2$), separted by a plane boundary, are subjected to a constant acceleration g normal to the interface with direction from fluid 2 to fluid 1.

In the absence of viscosity the amplitude, a, of a small sinusoidal perturbation of wavelength λ grows according to the formula, see Chandrasekhar [1]

$$a = a_0^+ \exp(n_\lambda t) + a_0^- \exp(-n_\lambda t) . \tag{1}$$

The growth rate n_λ is given by

$$n_\lambda^2 = \frac{2\pi g}{\lambda} \frac{\rho_1 - \rho_2}{\rho_1 + \rho_2} . \tag{2}$$

Consider the case when many different wavelength components are present. According to eqn (2) short wavelength small perturbations grow more rapidly than long wavelength small perturbations. When the amplitude of the perturbation becomes significant compared to its wavelength the rate at which the instability penetrates the denser fluid approaches a limiting value proportional to $\sqrt{g\lambda}$, see Lewis [8]. Short wavelength perturbations then grow more slowly than long wavelength perturbations. The result of this behaviour is that one expects small structures to appear first. As time proceeds larger and larger structures should dominate the flow. The way in which the dominant wavelength increases, by bubble competition, was obseved in the experiments of Lewis [8] and Emmons et al. [9]. If a bubble of the lighter fluid penetrating the denser fluid is slightly larger than its neighbours it grows more rapidly and eventually crowds out the surrounding bubbles.

In the absence of viscosity or any other mechanism which stabilises the short wavelength perturbations, the growth rate, n_λ, increases without limit as the wavelength is decreased. However, if viscosity is present, n_λ reaches a maximum value ($=n_m$) corresponding to the most unstable wavelength λ_m. According to [1]

$$\lambda_m \approx 4\pi \left\{ \frac{\nu^2}{g} \frac{\rho_1 + \rho_2}{\rho_1 - \rho_2} \right\}^{1/3}$$

and

$$n_m = \left\{ \frac{\pi g}{\lambda_m} \frac{\rho_1 - \rho_2}{\rho_1 + \rho_2} \right\}^{1/2} ,$$

where

$$\nu = \frac{\mu_1 + \mu_2}{\rho_1 + \rho_2} \tag{3}$$

is the mean kinematic viscosity.

The evolution of larger and larger structures should begin with the appearance of perturbations with wavelength of order λ_m.

The phenomenon appears to be analogous to that seen in a number of turbulent shear flows such as the plane mixing layer, see ref. 10 for example. Here, larger and larger structures appear as fluid is carried downstream. An important feature of this flow is that memory of the initial conditions tends to be lost as the downstream distance increases. Then, as expected from dimensional analysis, the time averaged mixing profile at a given downstream station is described by a similarity solution with length scale equal to the distance downstream from the point of initiation of the mixing process.

These arguments suggest that the evolution of Rayleigh–Taylor instability at a plane boundary from a low initial perturbation level should give

rise to the following three stages of mixing:

Stage 1. A perturbation corresponding to the most unstable wavelength λ_m appears. This should happen after a time of a few times τ_m where $\tau_m = 1/n_m$.

Stage 2. When the perturbation of wavelength λ_m reaches a height of the order of $\frac{1}{2}\lambda_m$ its exponential growth rate slows down and longer wavelength perturbations begin to grow more rapidly. In stage 2 larger and larger structures appear. If the initial perturbation level is low enough, these larger structures will evolve from the non-linear interaction between smaller structures rather than directly from an initial perturbation of the corresponding wavelength. Then by the end of stage 2 memory of the initial conditions will be lost. This should occur when the dominant wavelength λ_d reaches about $10\lambda_m$.

Stage 3. In stage 3, λ_d, grows from about $10\lambda_m$ to infinity. Viscosity now has little effect on the growth of the large-scale features. Since memory of the initial conditions has been lost, gt^2 is the only length scale of importance. For a given density ratio the mixing process is described by a similarity solution with length scale proportional to gt^2. The width of the mixed region is given by

$$\delta = F\left(\frac{\rho_1}{\rho_2}\right)gt^2 . \tag{4}$$

If large amplitude long wavelength perturbations are present initially the growth of the mixed region will exceed that indicated by eq. (4).

The width δ could be defined in a variety of ways. One possibility is as follows. Let $f_1(x, y, z)$ denote the volume fraction of the dense fluid 1 at the point (x, y, z), z is measured in the direction normal to the interface. The plane average of f_1 at height z is

$$\bar{f}_1(z) = \int\int f_1(x, y, z)\,\mathrm{d}x\,\mathrm{d}y \Big/ \int\int \mathrm{d}x\,\mathrm{d}y .$$

The mixed region width, δ = difference in height between points where $\bar{f}_1 = 0.01$ and $\bar{f}_1 = 0.99$; the penetration of dense fluid, h_1 = difference in height between position undisturbed interface would have reached and point where $\bar{f}_1 = 0.99$; the penetration of light fluid, h_2 = difference in height between position undisturbed interface would have reached and point where $\bar{f}_1 = 0.01$. By definition $\delta = h_1 + h_2$.

A simple argument may be used to indicate the dependence on density ratio in eq. (4). Suppose that throughout stage 3 of the mixing process the dominant wavelength takes N exponential growth periods to appear, so that

$$n_{\lambda_d} t = N = \text{a constant.}$$

Then

$$\delta \propto \lambda_d = \frac{2\pi}{N^2}\frac{\rho_1 - \rho_2}{\rho_1 + \rho_2} gt^2 \tag{5}$$

by using eq. (2).

Computer simulation and experimental results both show that the density variation in eq. (5) is more applicable to h_1, the penetration of the denser fluid, than to δ the total width.

2.2. *Computer simulation of the growth of the instability from a single wavelength initial perturbation*

Although multiple wavelength initial perturbations are of most interest, it is instructive to begin by considering the growth of the instability from a single sinusoidal perturbation. In the computer simulation, fluid of density ρ_1 rests initially on top of fluid of density ρ_2. Gravity acts downwards. The interface between the two fluids is initially horizontal but a velocity perturbation is present. This is a combination of the eigenfunctions (at $t = 0$) obtained from the linear theory, corresponding to the case $a_0^+ = -a_0^- = 0.5a_0$ in eq. (1). The stream function is $\psi = -(a_0 n/k)\sin kx \exp(-k|z|)\cosh nt$, where x and z are the distances in the horizontal and vertical directions. The displacement of the interface, ac-

cording to linear theory is then

$$\zeta(x) = \int -\frac{\partial \psi}{\partial x}\bigg|_{z=0} \mathrm{d}t = a_0 \cos kx \sinh nt. \qquad (6)$$

Simulations have been performed using the 2-D Eulerian compressible flow code of Youngs [11]. Equations of state were chosen to give a low Mach number flow. The effect of compressibility on the results is then negligible. An interface tracking method is used to follow the boundary between the two fluids. In each mixed cell, fluid volume fractions for the cell under consideration and its eight neighbours are used to construct a straight-line interface. This type of interface tracking method was first used by DeBar [12].

Fig. 1 shows calculations at density ratios of $\rho_1/\rho_2 = 3$ and 20. Gravity is chosen so that $g(\rho_1 - \rho_2)/(\rho_1 + \rho_2)$ is the same in each case. The penetration of the denser fluid, h_1, then grows at a similar rate for the two density ratios (growth is in fact a little more rapid at $\rho_1/\rho_2 = 3$). At $\rho_1/\rho_2 = 3$, as the spike of denser fluid falls, the interface soon rolls up. This phenomenon was first computed by Daly [13]. The present calculations show that a similar process happens at $\rho_1/\rho_2 = 20$ but at a larger value of nt. At the larger density ratio, the asymmetry of mixed region, h_2/h_1, is greatly increased. The spike penetration, h_2, does, however fall a long way short of the free-fall line $h_2 = \frac{1}{2}gt^2$. At the latest time shown in fig. 1, h_2 is only $0.35 \times \frac{1}{2}gt^2$.

2.3. *Computer simulation of the growth of the instability from a multiple wavelength initial perturbation*

The multiple wavelength calculations require a large number of computational meshes. In order to carry out such calculations a numerical technique was devised which was simpler than that used for the single wavelength instability calculations. An incompressible hydrocode somewhat similar to the MAC code, [14] was written. As a high degree of fine scale mixing was expected, the interface tracking method was abandoned. Instead, the fluid volume fraction, f_1, is treated as a continuous function of position. Changes in f_1 are calculated by solving the advection equation

$$\frac{\partial f_1}{\partial t} + \mathrm{div}(f_1 \boldsymbol{u}) = 0.$$

The monotonic advection method of Van Leer [15] is used. The method (which is also used in the advection phase of the compressible code [11]) gives minimal numerical diffusion whilst ensuring that the values of f_1 remain in the interval [0, 1].

For the Rayleigh–Taylor instability calculations

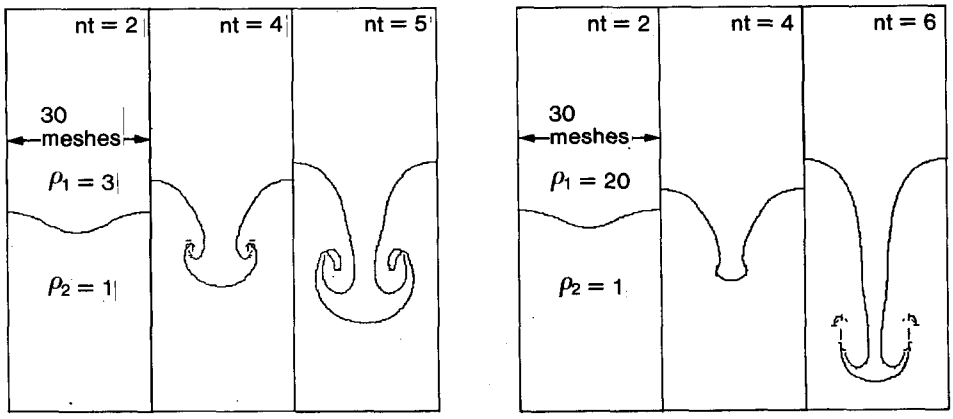

Fig. 1. Rayleigh–Taylor instability, single wavelength initial perturbation.

shown here, where flow is confined to the region $0 \leqslant x \leqslant L$, the initial velocity perturbation is derived from the stream function

$$\psi = -\sum_r a_r \frac{n_r}{k_r} \cos k_r x \exp(-k_r|z|), \quad k_r = \frac{r\pi}{L}.$$

Examples of two such calculations are shown in fig. 2. The initial perturbation, the same for each case consists of 12 modes with $r = 49$ to 60. The values of a_r were chosen at random from a Gaussian distribution. Viscosity is present in these calculations. Fluid viscosities are chosen so that the most unstable wavelength λ_m is equal to $L/100$. Viscosity then has little effect on the large scale features that are formed by the end of the calculation. In the calculations shown here $L = 1$ unit and $g(\rho_1 - \rho_2)/(\rho_1 + \rho_2)$ has the same value at the two density ratios; g is in fact chosen so that the exponential growth rate, n, is unity for wavelength L. It is then found that the penetration of the dense fluid, h_1, grows at a similar rate for the two density ratios. In these calculations the dominant wavelength increases from $\approx L/30$ at the beginning of the calculation to $\approx L/3$ at the end of the calculation. Perturbations of wavelength $L/3$ are not present initially. Hence these structures must have been formed from the non-linear interaction between smaller structures. In these circumstances it is expected that the average mixing rate, i.e. that deduced from the profile of $\bar{f}_1$ versus z, should be insensitive to the initial conditions. This is found to be the case. For the calculations shown here and

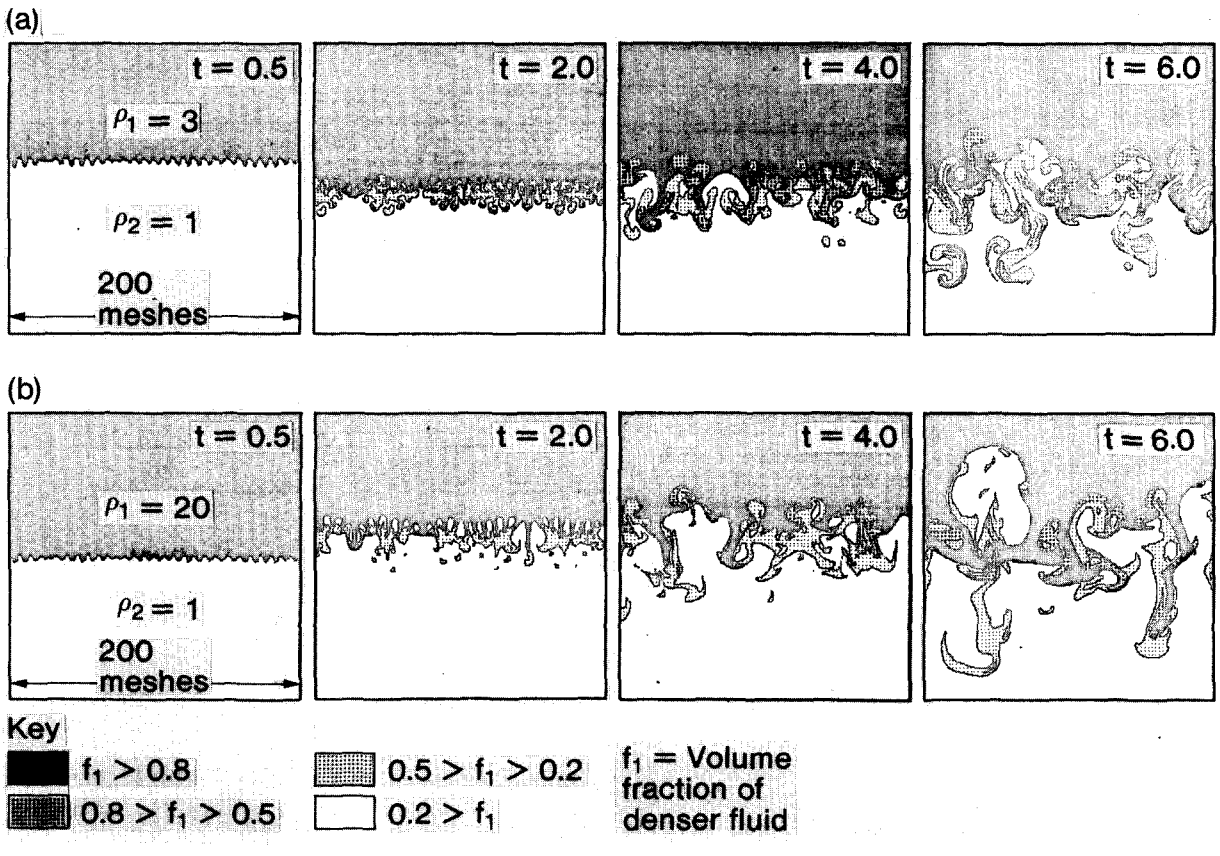

Fig. 2. Rayleigh–Taylor instability, multiple wavelength initial perturbation.

others with different initial conditions:

$$h_1 = \alpha \frac{\rho_1 - \rho_2}{\rho_1 + \rho_2} g t^2 , \tag{7}$$

where

$\alpha \approx 0.04$ to 0.05.

Eq. (7) was confirmed by experimental investigation [6, 7]. For experiments in which the instability evolved from small random perturbations and developed uniformly over the interface, good linear correlations were obtained between h_1 and gt^2. Values of α for the three dimensional experiments were in the range 0.063 to 0.077. The experimental estimates of α tend to be higher than the values from the two-dimensional calculations. It is argued in [6] that two-dimensional constraints inhibit the growth of the large scale structures.

Fig. 3 shows plots of the average volume fraction $\bar{f}_1$ versus z obtained from the calculations illustrated in fig. 2. For each density ratio the shape of the volume fraction profile remains similar as the mixed region grows. The ratio h_2/h_1 increases as the density ratio increases:

$\rho_1/\rho_2 = 3, \quad h_2/h_1 \approx 1\frac{1}{2},$

$\rho_1/\rho_2 = 20, \quad h_2/h_1 \approx 2\frac{1}{2}.$

The calculation shown in fig. 2a was repeated with an additional perturbation of wavelength $L/2$. This long wavelength initial velocity perturbation was chosen to make the interface displacement, as given by eq. (6)

$\zeta(x) = 0.01L \cos kx \sinh nt .$

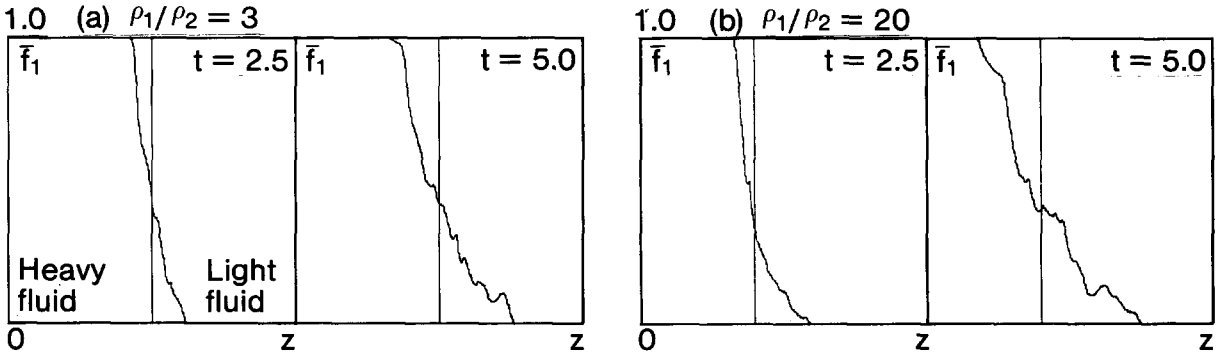

Fig. 3. Dense fluid volume fraction averaged over horizontal layers, $\bar{f}_1$, plotted against depth z.

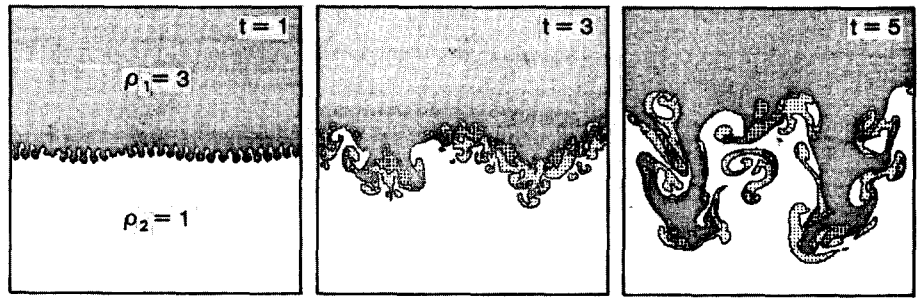

Fig. 4. Multiple wavelength calculation shown in fig. 2(a) repeated with an additional long wavelength initial perturbation.

The effect is very similar to that of introducing an amplitude perturbation, with zero initial velocity, for which the initial growth is given by

$$\zeta(x) = 0.01L \cos kx \cosh nt .$$

In this case the initial amplitude is 2% of the wavelength.

The addition of this long wavelength perturbation increases the instability penetration, h_1, by about 50% towards the end of the calculation, see fig. 4. On the other hand, if the size of the perturbation is reduced by a factor 10, so that it corresponds to an initial amplitude of 0.2% of the wavelength, the enhancement of the instability is negligible.

The quadratic law, eq. (7) will therefore cease to be valid if large amplitude long wavelength perturbations are initially present.

3. Richtmyer–Meshkov instability

3.1. *Small amplitude theory*

Mixing induced by the transit of shocks normal to the interface is now considered. Firstly, the small amplitude results of Richtmyer [2] are noted. Consider the growth of an initial amplitude perturbation at an interface between two incompressible fluids, i.e. $a_0^+ = a_0^- = \frac{1}{2}a_0$ in eq. (1). After time t the amplitude and velocity are

$$a = a_0 \cosh nt ,$$

$$v = \dot{a} = na_0 \sinh nt .$$

If $t \to 0$ and $gt \to \Delta U$ in these equations the following results are obtained, for an impulsive acceleration with velocity change ΔU:

$$a = a_0, \quad v = \frac{2\pi \Delta U}{\lambda} a_0 \frac{\rho_1 - \rho_2}{\rho_1 + \rho_2} . \tag{8}$$

Richtmyer showed that eq. (8) gave a good approximation for the effect of a shock passing through the interface between compressible fluids provided that a_0, ρ_1 and ρ_2 were measured after the shock transit.

3.2. *The shock tube experiment*

Computer simulation has been used to investigate the shock tube experiment of Andronov et al. [3]. The experimental geometry is illustrated in fig. 5. The helium/air interface is first accelerated by a shock wave passing from the air to the less dense helium. This shock transit amplifies the perturbation introduced when the thin film which separates the two gases is ruptured. Subsequently the interface is decelerated by reflected shocks. Most of the mixing occurs in this deceleration phase. A region of turbulent mixing was observed and a visual estimate of its width as a function of time was obained [3]. The experiment was of course three dimensional; the shock tube had cross-section 40 × 120 mm. The two-dimensional computer calculations were confined to a region with width 50 mm normal to the direction of shock propagation.

3.3. *Computer simulation with a single wavelength initial perturbation*

The 2-D compressible Eulerian code [11] was adapted to simulate the shock tube experiment. Calculations were performed in plane geometry with x measured in the shock direction and y measured in the normal direction. A rectangular mesh was used. The y-direction mesh was fixed. The x-direction mesh moved with velocity $\bar{u} = \int u dy / \int dy$, so that in the absence of interface

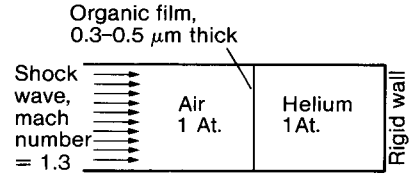

Fig. 5. Shock tube experiment, Andronov et al. [3].

perturbations, when the flow was one dimensional, the mesh moved in a Lagrangian manner. This maintained the resolution in the helium region as it compressed. Moving rectangular mesh methods have been used before, by Emery et al. [16], to improve the accuracy of Rayleigh–Taylor instability calculations. They are also discussed by Pert [17].

Fig. 6 shows the variation of the width of the helium reigon with time for a calculation with no interface perturbation. The graph shows the changes in the velocity at the interface due to shock transits. 80 meshes were used in the x-direction in the helium region. The helium and the air were treated as perfect gases with adiabatic constants $\gamma = 1.4$ and $\gamma = 1.63$, respectively. The density ratio, ρ_1/ρ_2, at the interface remained in the interval 7 to 8.

A two-dimensional calculation was carried out with the following initial amplitude perturbation at the interface:

$$\zeta(y) = a_0 \cos\frac{2\pi y}{\lambda},$$

with

$$a_0 = 1\ \text{mm} \quad \text{and} \quad \lambda = 50\ \text{mm}.$$

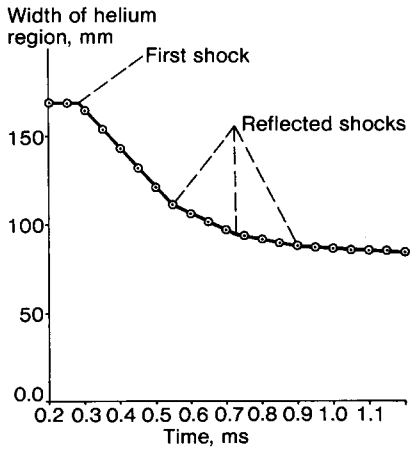

Fig. 6. Shock tube experiment; computer simulation with no interface perturbation.

Plots of the helium/air interface and vectors of the perturbed velocity $(u - \bar{u}, v)$ are shown in fig. 7. A total of 200×40 meshes are used. A uniform 80×40 mesh is initially present in the helium region. Then, at peak compression the mesh in the helium region is approximately square.

The first shock reaches the interface at 0.283 ms. As expected from eq. (8), since $\Delta U(\rho_1 - \rho_2)$ is negative, the sign of the perturbation is reversed. The computer simulation shows that for this shock $\Delta U = -220$ mm/ms. After the shock has passed

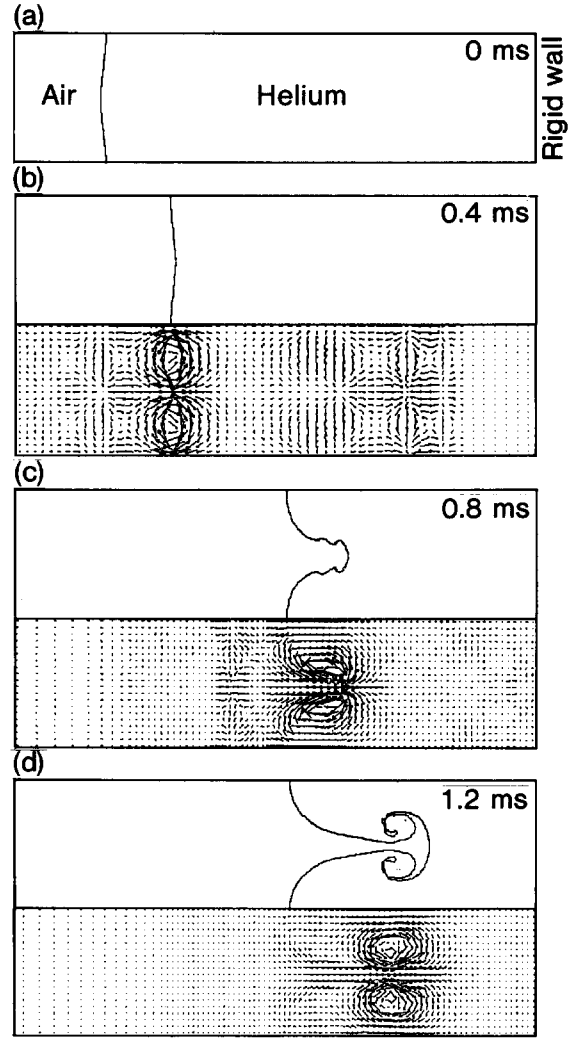

Fig. 7. Shock tube experiment with single wavelength initial perturbation at the helium/air interface.

$\rho_1/\rho_2 = 7.4$ and the fluid is compressed by a factor 1.3. Eq. (8) then gives

$$v = -\frac{2\pi \times 220}{50}\frac{1}{1.3}\frac{7.4-1}{7.4+1} = -16\,\text{mm/ms}.$$

The perturbation amplitude changes from +1 mm to −1 mm in about 0.12 ms (see fig. 8). This gives velocity $v \approx -2/0.12 = -17$ mm/ms in good agreement with Richtmyer's formula.

After the first shock has passed through the interface, perturbations are present on the shock front. This is demonstrated by the perturbation velocity vector plot in fig. 7 at 0.4 ms.

For the subsequent reflected shocks $\Delta U(\rho_1 - \rho_2)$ is positive. These shocks enhance the growth of the instability. Towards the end of the calculation, as the spike of air penetrates the less dense helium, the interface rolls up. The shape of the interface is in fact very similar to that seen in section 2.2 for Rayleigh–Taylor instability at a constant acceleration.

Fig. 8 shows the variation with time of the width of the instability for this calculation. The growth agrees reasonably well with the observed data. This agreement is somewhat fortuitous as the flow is not, in reality, dominated by the growth of a single wavelength perturbation.

3.4. *Computer simulation with a multiple wavelength initial perturbation*

A more realistic simulation of the shock tube experiment is obtained if the initial perturbation consists of a mixture of different wavelength modes. In order to achieve this the following interface perturbation was used:

$$\zeta(y) = \sum_{r=10}^{40} a_r \cos\frac{r\pi y}{W}.$$

The coefficients a_r were chosen from a Gaussian distribution. The width of the computational region in the y-direction, W, was 50 mm. The range of wavelengths present in the initial perturbation was $2\frac{1}{2}$ to 10 mm. The magnitude of the perturbation was scaled to make the standard deviation $\overline{(\zeta^2)}^{1/2} = 0.2$ mm.

The calculation was performed with 370 meshes in the x-direction and 100 meshes in the y-direction. As it was anticipated that fine scale mixing would occur in some regions, the interface

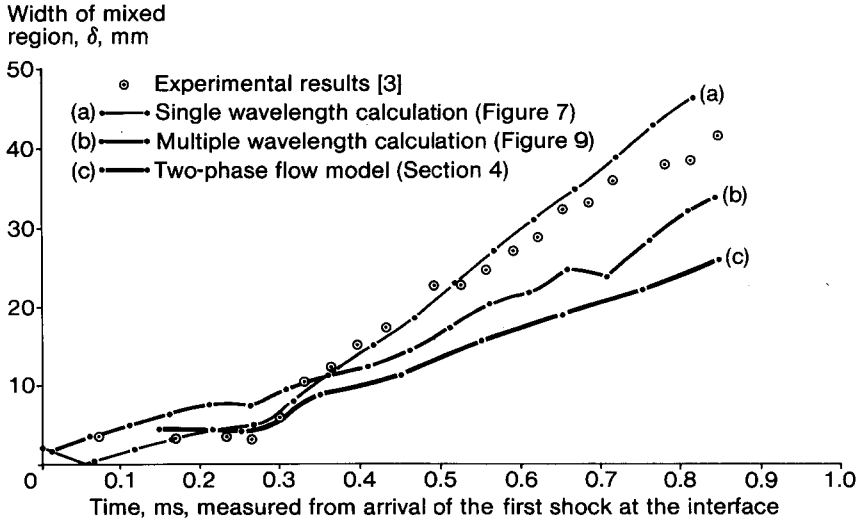

Fig. 8. Shock tube experiment, growth of the mixed region.

tracking method was modified. A straight line interface was only defined in a mixed cell if one of its eight neighbours was pure i.e. all helium or all air. If all the surrounding eight cells were mixed, it was assumed that the volume fractions varied continuously with position and the Van Leer method was used to calculate transport across cell sides as in the calculations described in section 2.3.

Fig. 9 shows plots of the helium/air interface, perturbation velocity vectors $(u - \bar{u}, v)$ and air volume fraction contours. Cells where the interface tracking method has not been used are marked with a + on the interface plot. The results show that, as in the Rayleigh–Taylor calculations of section 2.3, the dominant wavelength associated with the instability increases as the mixed region grows. Initially λ_d is about $3\frac{1}{2}$ mm. By the end of the calculation λ_d has increased to about 15 mm.

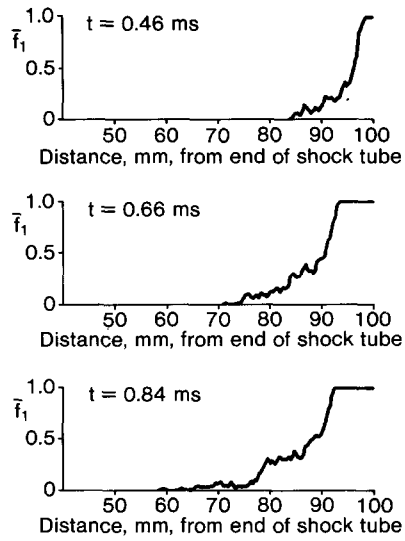

Fig. 10. Mean air volume fraction profiles for the shock tube experiment. Multiple wavelength instability calculation. Times are measured from the arrival of the first shock at the interface.

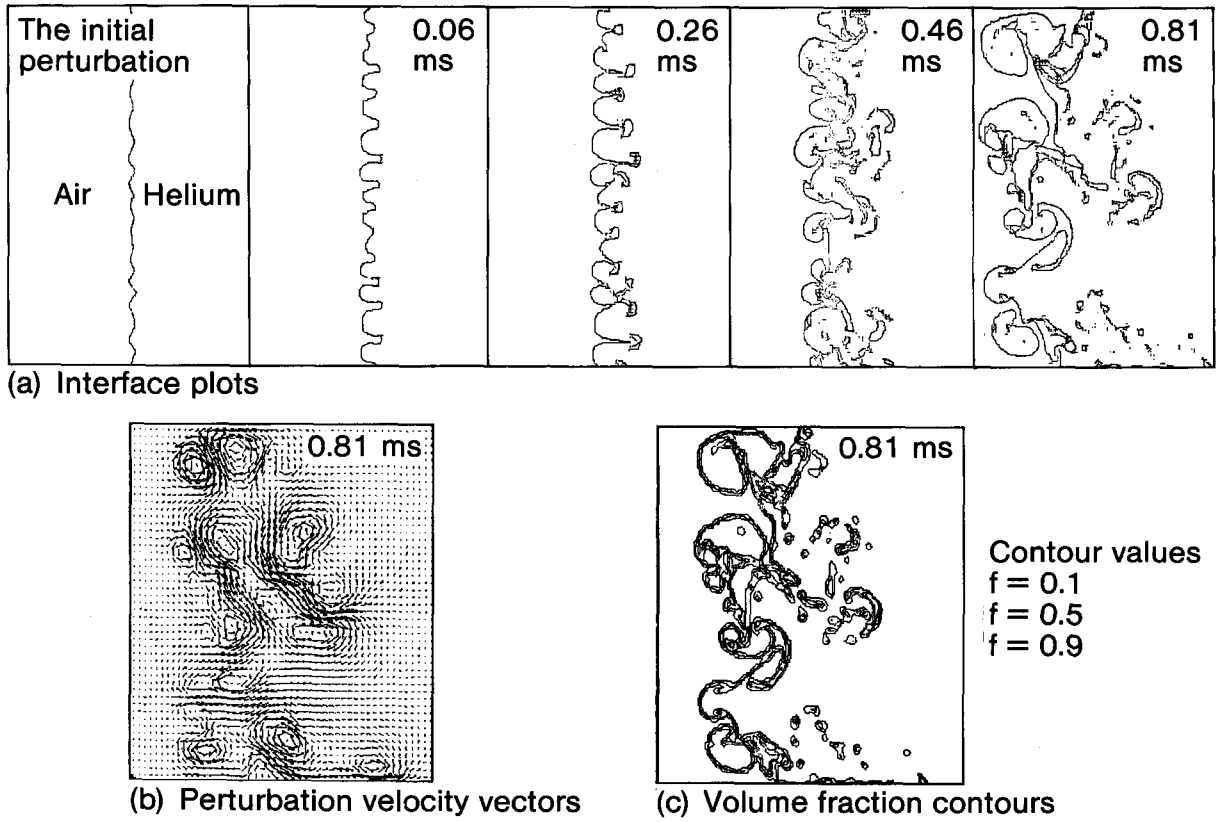

Fig. 9. The multiple wavelength instability calculation for the shock tube experiment. Times are measured from the arrival of the first shock at the interface.

Profiles of the mean air volume fraction, $\bar{f}_1 = \int f_1 \, dy / \int dy$ are shown in fig. 10. The shapes obtained are similar to those for Rayleigh–Taylor instability with constant acceleration. The width, δ, of the mixed region i.e. the distance between the points where $\bar{f}_1 = 0.99$ and $\bar{f}_1 = 0.01$ is plotted in fig. 8. Towards the end of the calculation the growth of the mixed region is less than observed. This may be due to the fact that the simulation is two-dimensional whereas the experiment was three dimensional.

4. Empirical models

The two dimensional calculations of multiple wavelength instability growth described in sections 2.3 and 3.4 each took about two hours on a CRAY-1 computer. For the more complex geometries present in real applications, such calculations would be impractical in two dimensions, out of the question in three dimensions. Simple empirical models are therefore needed to assess the effects of interface break up in these situations. Such a model would not attempt to predict the mixing processes from first principles. Instead it should be thought of as a way applying the results of experiments and computer simulation in simple situations, to real problems.

Andronov et al. [3] described a one-dimensional model for the mixing process in the shock tube experiment. Mixing of the two gases was represented by turbulent diffusion. The mass flux of fluid 1 was

$$F_1 = -\rho D_t \frac{\partial c_1}{\partial x},$$

where c_1 is the concentration, per unit mass, of fluid 1.

The coefficient of turbulent diffusion was

$$D_t = \text{a constant} \times k^{1/2} L,$$

where k is the turbulence kinetic energy and L is the width of the mixed region.

An alternative approach is suggested here. The mixed region grows because, within the mixed region, the pressure gradient induces different accelerations in the two fluids which have different densities. The difference in the velocities of the two fluids is limited by drag, as in the case of a single gas bubble rising in a liquid when gravity is present. This behaviour suggests that the two-phase flow equations, see for example [18], should be used to model the process. Some preliminary calculations have been carried out with the following simple one dimensional two-phase flow model:

mass conservation:

$$\frac{\partial}{\partial t}(f_r \rho_r) + \frac{\partial}{\partial x}(f_r \rho_r u_r) = 0, \quad r = 1 \quad \text{and} \quad 2;$$

momentum conservation:

$$\frac{\partial}{\partial t}(f_r \rho_r u_r) + \frac{\partial}{\partial x}(f_r \rho_r u_r^2) = -f_r \frac{\partial p}{\partial x} + K(u_s - u_r) + f_r \rho_r g,$$

$r = 1$ and 2, $s = 2$ and 1.

f_r, ρ_r and u_r denote the volume fraction, density and velocity of fluid r averaged over planes perpendicular to the x direction. For compressible flows, internal energy equations for each fluid, see [18], are also solved. The interphase drag coefficient used here has the following form:

$$K = C \frac{f_1 f_2 \bar{\rho}}{L} |u_1 - u_2|, \tag{9}$$

where

$$\bar{\rho} = f_1 \rho_1 + f_2 \rho_2$$

and

C = a constant.

The length scale L, which in this model depends only on t, is proportional to the dominant bubble

or drop radius at time t. It is assumed to grow in proportion to the width of the mixed region. This is appropriate to the case when the instability evolves from small random perturbations.

The equation used for L was

$$\frac{\mathrm{d}L}{\mathrm{d}t} = V_0 + L\left(\frac{\partial \bar{u}}{\partial x}\right)_0,$$

where V_0 is the value of $|u_1 - u_2|$ at the centre of the mixed region. The velocity gradient term $(\partial \bar{u}/\partial x)_0$ ensures that, in the absence of velocity separation, the length scale is compressed when the fluid is compressed.

Further work needs to be done to perfect this model. It could be extended to deal with two dimensional problems where the average values $f_r, \rho_r, u_r \ldots$ are functions of two space variables. A more sophisticated length scale equation would then be needed. Although it is suggested here that gradient diffusion by itself does not represent the mixing process well, such effects may need to be included in the model. The interphase drag is a source of turbulence kinetic energy. In periods where the pressure gradient falls to zero this may cause the fluids to mix in a manner similar to gradient diffusion. For the transient flows considered here it is likely that added mass terms, as described by Ishii and Chawla [9] for example, need to be included in the momentum equations.

Results obtained with the simple model described here are now discussed. It has been applied to mixing at the interface between two incompressible fluids subject to constant acceleration g. If the constant in the drag formula (9) is chosen to be $C = 4.5$, then the penetration of the dense fluid given by

$$h_1 = \beta \frac{\rho_1 - \rho_2}{\rho_1 + \rho_2} g t^2,$$

where β varies only slightly with density ratio. At $\rho_1/\rho_2 = 8$, $\beta = 0.07$ in agreement with the experimental results [6].

Volume fraction profiles obtained from calculations at $\rho_1/\rho_2 = 3$ and 20 are shown in fig. 11. The shapes obtained agree well with those indicated by the numerical simulation of section 2.3.

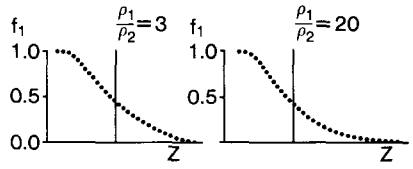

Fig. 11. Volume fraction profiles predicted by the two phase flow model for the mixing of two incompressible fluids.

The two-phase flow model has also been applied to the shock tube experiment. The present model does not cope with the reversal and amplification of the initial perturbation by the first shock. The mixing calculation was started just after the first shock had passed through the interface, with a mixed region 4 mm wide as observed in the experiment. The length scale L was initially set equal to 2 mm. A one-dimensional Lagrangian code was used; the Lagrangian mesh moved with the mean fluid velocity $\bar{u} = f_1 u_1 + f_2 u_2$. Profiles of the air volume fraction at a series of times are shown in fig. 12. Again, it is found that the shapes predicted by the model agree with those obtained from the

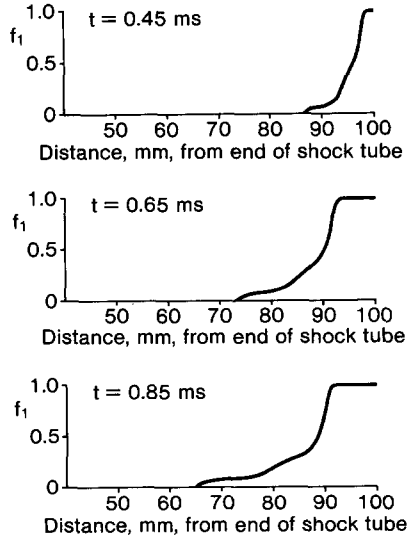

Fig. 12. Air volume fraction profiles for the shock tube experiment predicted by the two-phase flow model. Times are measured from the arrival of the first shock at the interface.

two-dimensional instability calculation, fig. 10. The width, δ, of the mixed region predicted by the model does not grow as fast as observed, see fig. 8. It does, however, grow at a similar rate to that in the two-dimensional numerical simulation of the shock tube experiment.

The tie-up between application of the model to the constant acceleration case and the shock tube experiment is not as good as one would like. It is not clear at present if this is due to inadequacies in the model or difficulties in interpreting the experiments. More precise measurements of the amount of mixing in the experiments, for example measurement of the mean volume fraction profiles would be invaluable.

5. Conclusions

As already noted, most of the past research into Rayleigh–Taylor instability, both theoretical and experimental, has investigated the growth of a single wavelength perturbation. At first sight, extending the research to cope with multiple wavelength initial perturbations seems a daunting task. However, there are compensations. If the mixing process evolves from small random perturbations then the growth of the instability is soon controlled by the nonlinear interaction between bubbles of different sizes. It is then found that the mixing rate is insensitive to the initial conditions, which are rarely known in a real situation. Also, numerical simulation of mixing at a plane boundary has shown that the average properties of the mixed region, such as the volume fraction ($\bar{f}_1$) profiles, then fit into a simple pattern.

Much further work needs to be done. In the author's opinion the most effective way to proceed is to extend the understanding of the mixing process by the use of two-dimensional computer simulation and three-dimensional experiment. Simple empirical models should then be used to apply the results obtained to real situations.

References

[1] S. Chandrasekhar, Hydrodynamic and Hydromagnetic Stability (Oxford Univ. Press, Oxford, 1961).
[2] R.D. Richtmyer, "Taylor Instability in Shock Acceleration of Compressible Fluids", Comm. in Pure and Appl. Math. 13 (1960) 297.
[3] V. Andronov, S.M. Bakhrakh, E.E. Meshkov, V.N. Mokhov, V.V. Nikiforov, A.V. Pevnitskii and A.I. Tolshmyakov, Sov. Phys. JETP 44 (1976) 424–427.
[4] P.D. Roberts, S.J. Rose, P.C. Thompson and R.J. Wright, "The Stability of Multiple Shell ICF Targets", J. Phys D 13 (1980) 1957.
[5] D.H. Sharp, "An Overview of Rayleigh-Taylor Instability", Physica 12D (1984) 3 (these proceedings).
[6] K.I. Read, "Experimental Investigation of Turbulent mixing by Rayleigh-Taylor Instability", Physica 12D (1984) 45 (these proceedings).
[7] K.I. Read and D.L. Youngs, "Experimental Investigation of Turbulent Mixing by Rayleigh–Taylor Instability", AWRE Report 011/83 (1983).
[8] D.J. Lewis, The Instability of Liquid Surfaces when Accelerated in a Direction Perpendicular to their Plane", Proc. Roy. Soc. 202A (1950) 81.
[9] H.W. Emmons, C.T. Chang and B.C. Watson, "Taylor Instability of Finite Surface Waves", J. Fluid Mech. 7 (1963) 177.
[10] G.L. Brown and A. Roshko, "On Density Effects and Large-Scale Structure in Turbulent Mixing Layers", J. Fluid Mech. 64 (1974) 775.
[11] D.L. Youngs, "Time-Dependent Multi-Material Flow with Large Fluid Distortion", in: Numerical Methods for Fluid Dynamics, K.W. Morton and M.J. Baines, eds. (Academic Press, New York, 1982).
[12] R. DeBar, "A Method in Two-D Eulerian Hydrodynamics", UCID-19683 (1974).
[13] B.J. Daly, "Numerical Study of Two Fluid Rayleigh–Taylor Instability", Phys. Fluids 10 (1967) 297.
[14] J.E. Welch, F.H. Harlow, J.P. Shannon and B.J. Daly, "The MAC Method: a Computing Technique for Solving Viscous Incompressible Transient Fluid Flow Problems Involving Free Surfaces", LA-3425 (1966).
[15] B. van Leer, "Towards the Ultimate Conservative Difference Scheme: IV, A New Approach to Numerical Convection", J. Comp. Phys. 23 (1977) 276.
[16] M.H. Emery, J.H. Gardner and J.P. Boris, "Rayleigh–Taylor and Kelvin–Helmholtz Instabilities in Targets Accelerated by Laser Ablation", Phys. Rev. Lett. 48 (1982) 677.
[17] G.J. Pert, "Quasi-Lagrangian Rezoning of Fluid Codes Maintaining an Orthogonal Mesh", J. Comp. Phys. 49 (1983) 1.
[18] F.H. Harlow and A.A. Amsden, "Numerical Calculation of Multiphase Fluid Flow", J. Comp. Phys. 17 (1975) 19.
[19] M. Ishii and T.C. Chawla, "Local Drag Laws in Dispersed Two-phase Flow", NUREG/CR-1230 (1979).